Progress In Electromagnetics Research M, Vol. 20, 155–169, 2011

PROPERTIES OF ENVELOPE PULSES DEVELOPED IN COUPLED NONLINEAR COMPOSITE RIGHT- AND LEFT-HANDED TRANSMISSION LINES

K. Narahara*

Graduate School of Science and Engineering, Yamagata University, 4-3-16 Jonan, Yonezawa, Yamagata 992-8510, Japan

Abstract—We investigate the properties of nonlinear envelope pulses developed in a coupled composite right- and left-handed (CRLH) transmission line with regularly spaced Schottky varactors. It is found that the dispersive distortion of the envelope pulses carried by each mode is well compensated by nonlinearity introduced by the varactors. In addition, we numerically observe that the collision of two nonlinear envelope pulses leads to the development of a new pair of envelope pulses (one traveling forward and the other backward). The newly developed pulses become maximal when phase-matching with the original pulses is established, and their carrier frequency is close to that of the harmonics of the colliding pulses.

1. INTRODUCTION

Composite right- and left-handed (CRLH) transmission lines have been investigated for their unique electromagnetic [1] and dispersive properties [2, 3]. A CRLH line also attracts considerable attention for pulse management [4]. In particular, pulse propagation in nonlinear CRLH lines has been well investigated, including purely left-handed transmission lines with series varactors [5–9] and CRLH lines with shunt varactors [10, 11]. In general, a broadband pulse cannot travel on the CRLH line without distortion, because the line exhibits high dispersion. As a result of the balance between the dispersion and the nonlinearity introduced by the varactors, undistorted envelope pulses governed by the nonlinear Schrödinger (NS) equation can be developed. Recently, we numerically investigated the collision of such nonlinear envelope pulses and found that a pair of envelope pulses was

Received 27 July 2011, Accepted 22 August 2011, Scheduled 29 August 2011

* Corresponding author: Koichi Narahara (narahara@yz.yamagata-u.ac.jp).

Table 1. Comparison between Schottky CRLH line (single) and coupled Schottky CRLH line (coupled).

	Single	Coupled
Collision-generated pulses	+	+
Mode conversion	−	+
Impedance conversion	±	+
Design facility	+	−
Potential for loss compensation	−	+

newly developed, one traveling forward and the other backward [12]. This mechanism can potentially be used to manage the directivity of radiating waves because the line operates as a leaky-wave antenna.

To enhance the potential of the nonlinear envelope pulses, we investigate two coupled CRLH lines, one of which is periodically loaded with Schottky varactors, called coupled Schottky CRLH lines for brevity. Owing to the coupling, maximum two different modes exist at a given frequency. Table 1 compares the coupled Schottky CRLH line with the Schottky CRLH line. The number of components required for the coupled Schottky CRLH line is nearly twice as much as that for the Schottky CRLH line. In return for this complexity, the coupled Schottky CRLH line has several advantages over the Schottky CRLH line. In the case of the coupled Schottky CRLH line, it is found that each mode can support nonlinear envelope pulses, whose pulse widths and amplitude fractions between the lines are uniquely determined by the dispersion and nonlinearity coefficients obtained for a given mode. Moreover, we numerically investigate the collisions of oppositely traveling nonlinear envelope pulses. We observe that the collision leads to the development of a new pair of envelope pulses similar to the Schottky CRLH lines. The newly developed pulses become maximal when phase-matching with the original pulses is established, and their carrier frequency is close to that of the harmonics of the colliding pulses. Moreover, the mode supporting the newly developed pulses is generally different from that of the original pulses. Obviously, this mode conversion is the unique property that the coupled Schottky CRLH line exhibits. This property results in the conversions of the voltage fraction between the lines and the characteristic impedance, which are uniquely determined by the mode. In addition, the coupled Schottky CRLH line has a potential to amplify the collision-generated envelope pulses. The large parasitic resistance of the inductor greatly diminishes the amplitude of the waves on the line, making the varactor's nonlinearity inefficient in compensating for

the dispersion of the CRLH lines. To cancel the wave attenuation, we consider a traveling-wave field-effect transistor (TWFET), whose gate and drain transmission lines have a CRLH line structure [13]. The gate and drain lines are coupled via the FET's drain-to-gate capacitance; therefore, the coupled Schottky CRLH line can be regarded as a pinch-off TWFET. Then, we can easily introduce the FET's gain to the coupled Schottky CRLH line, when we recognize lines 1 and 2 as the gate and drain lines, respectively, and take the contributions of the drain-to-source currents into considerations.

We first describe the circuit configuration and the dispersive properties of the coupled Schottky CRLH lines. Next, we discuss the predictions of the NS equation that perturbatively models the line and the results of several numerical time-domain calculations. Further, we explain the collision of two identical nonlinear envelope pulses to characterize the pulses newly developed by the collision. Moreover, we determine the properties of the newly developed pulses including wave numbers, carrier frequencies, and carrying modes. Finally, we describe several observations of the collision of two distinct nonlinear envelope pulses.

2. COUPLED SCHOTTKY CRLH LINES

Figure 1 shows a unit cell of the investigated line. Parameters L_{R1}, C_{L1}, and L_{L1} are the series inductance, series capacitance,

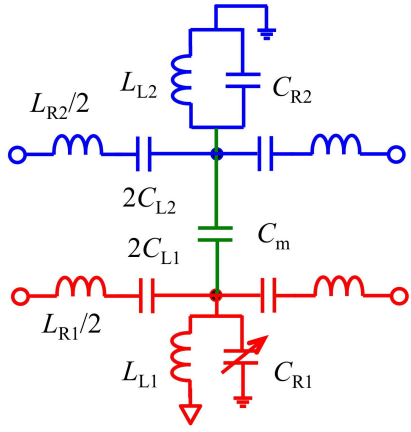

Figure 1. Equivalent circuits for unit cell of coupled Schottky CRLH lines. Red and blue elements represent lines 1 and 2, respectively. Lines 1 and 2 are coupled via mutual capacitance C_m.

and shunt inductance of line 1, respectively. The elements denoted with subscript 2 correspond to line 2. Lines 1 and 2 are coupled via mutual capacitance C_m. The shunt capacitances of lines 1 and 2 are represented by C_{R1} and C_{R2}, respectively. As the source of nonlinearity, the Schottky varactor is employed for C_{R1}. Its capacitance-voltage relationship is defined as

$$C_{R1}(V) = \frac{C_0}{\left(1 - \frac{V}{V_J}\right)^{m_J}}, \tag{1}$$

where C_0, V_J, and m_J are the zero-bias junction capacitance, junction potential, and grading coefficient, respectively. Hereafter, the biasing voltage of the Schottky varactor is represented by V_0. Using this representation, the transmission equations are given by

$$\frac{d^2 I_n}{dt^2} = -\frac{1}{L_{R1}} \left\{ \frac{I_n}{C_{L1}} + \frac{d}{dt}\left(V_n - V_{n-1}\right) \right\}, \tag{2}$$

$$\frac{d^2 J_n}{dt^2} = -\frac{1}{L_{R2}} \left\{ \frac{J_n}{C_{L2}} + \frac{d}{dt}\left(W_n - W_{n-1}\right) \right\}, \tag{3}$$

$$\begin{aligned} \frac{d^2 W_n}{dt^2} &= \frac{C_{R1} + C_m}{C_m} \frac{d^2 V_n}{dt^2} + \frac{V_n}{C_m L_{L1}} - \frac{1}{C_m} \frac{d}{dt}\left(I_n - I_{n+1}\right) \\ &\quad + \frac{1}{C_m} \frac{dC_{R1}}{dV_n} \left(\frac{dV_n}{dt}\right)^2, \end{aligned} \tag{4}$$

$$\frac{d^2 V_n}{dt^2} = \frac{C_{R2} + C_m}{C_m} \frac{d^2 W_n}{dt^2} + \frac{W_n}{C_m L_{L2}} - \frac{1}{C_m} \frac{d}{dt}\left(J_n - J_{n+1}\right), \tag{5}$$

where I_n, J_n, V_n, and W_n are the current on line 1 at the nth cell, the current on line 2 at the nth cell, the voltage on line 1 at the nth cell, and the voltage on line 2 at the nth cell, respectively.

We first linearize Equations (2)–(5) to examine the dispersive property of the line. Because the line has a very complicated structure, any characterizing expression are extremely complex; therefore, we hereafter confine the discussion to a coupled Schottky CRLH line with

Table 2. Line parameters of investigated line.

L_{R1} (nH)	1.5	L_{R2} (nH)	1.0
C_{L1} (pF)	2.4	C_{L2} (pF)	1.0
L_{L1} (nH)	1.2	L_{L2} (nH)	2.5
$C_{R1}(V_0)$ (pF)	2.0	C_{R2} (pF)	3.0
C_m (pF)	1.0		

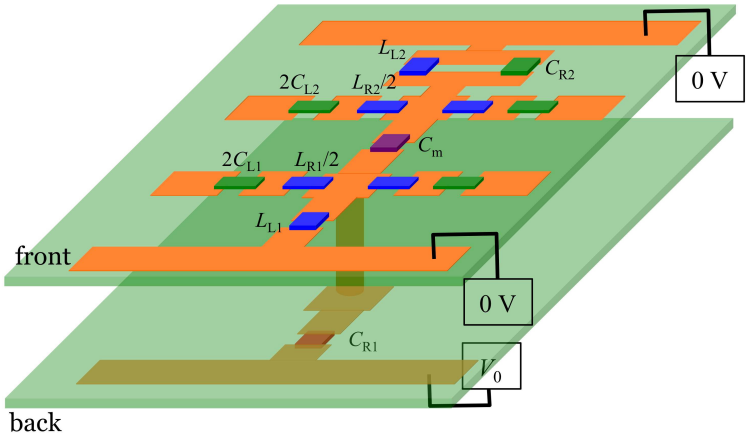

Figure 2. Sample structure of coupled Schottky CRLH lines.

the parameters listed in Table 2 for concise illustration. The main properties are precisely illustrated by the example listed in Table 2. We suppose that microwave surface-mount capacitors and inductors realize these line parameters and the print-circuit-board fabrication.

A sample structure of unit cell of a coupled Schottky CRLH line is shown in Figure 2. For the operating frequencies we investigate, the high frequency chip devices mounted on a glass epoxy board suit to fabricate the line. This sample configuration utilizes the double-sided print-circuit-board. The chip varactors are mounted on the back, while the other chip components are mounted on the front. Each node of line 1 is connected with the back wiring through a via hole to render the bias voltage to C_{R1}. Many manufacturers have the product line-ups of chip capacitor and inductor that include various electrical and geometrical properties, so that it is possible to select the size and reactance rather flexibly. Moreover, by minimizing the length of the wiring, its unfavorable contributions to the line's electrical properties can be reduced. The bias-dependent capacitance can also be implemented with surface-mount varactors. The minimum size of surface-mount chip inductor and capacitor is about 500 µm. Taking extra areas needed for solder coating into considerations, the unit cell size is practically 5.0 mm with allowance. The dispersion relationship is shown in Figure 3. Owing to the coupling, maximum two different modes exist for each frequency [14]. Note that modes 1 and 3 exhibit left-handed properties, while modes 2 and 4 exhibit right-handedness. Each mode has its own voltage fraction (line 2 voltage/line 1 voltage) between the lines denoted as R_i for mode i ($i = 1, 2, 3, 4$).

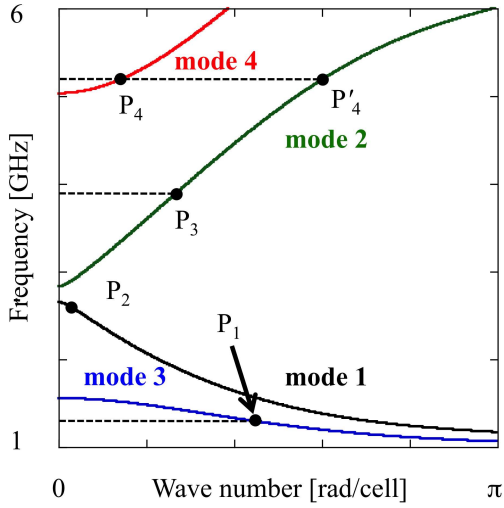

Figure 3. Dispersion of coupled Schottky CRLH lines.

3. PROPERTIES OF NONLINEAR ENVELOPE PULSES IN COUPLED SCHOTTKY CRLH LINES

To investigate the contribution of nonlinearity, we introduce spatial continuous variable x to define functions $V = V(x,t)$ and $W = W(x,t)$ as the continuous functions of voltages at the nth cell V_n and W_n, respectively. Moreover, we assign the respective spatial and temporal coordinates for the envelope and carrier waves. We use x and t as the spatial and temporal coordinates, respectively, for describing the carrier wave. For the envelope wave, $\xi \equiv \epsilon(x - U_g t)$ and $\tau \equiv \epsilon^2 t$ are used as the spatial and temporal coordinates, respectively, in which U_g represents the group velocity given by $\partial_k \omega(k)$, where $\omega = \omega(k)$ denotes the dispersion relationship for wave number k. Next, we expand the voltage variables as

$$V(x,t) = V_0 + \sum_{m_1=1}^{\infty} \epsilon^{m_1} \sum_{l=-\infty}^{\infty} v_l^{(m_1)}(\xi,\tau) e^{il(kx-\omega t)}, \tag{6}$$

$$W(x,t) = \sum_{m_1=1}^{\infty} \epsilon^{m_1} \sum_{l=-\infty}^{\infty} w_l^{(m_1)}(\xi,\tau) e^{il(kx-\omega t)}. \tag{7}$$

By applying the reductive perturbation method [15] to Equations (2)–(5), we obtain the NS equation that describes $w_1^{(1)}$:

$$i\partial_\tau w_1^{(1)} + p\partial_\xi^2 w_1^{(1)} + q\left|w_1^{(1)}\right|^2 w_1^{(1)} = 0, \tag{8}$$

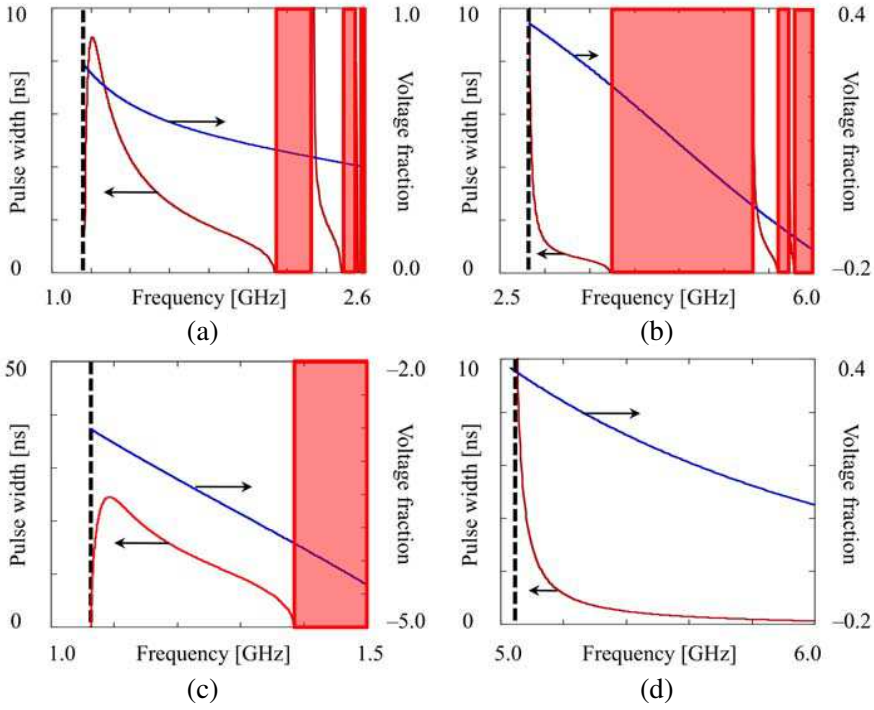

Figure 4. Pulse width and voltage fraction of a single bright soliton supported by each mode. Figures 4(a), (b), (c), and (d) correspond to modes 1, 2, 3, and 4, respectively. The bright solitons cannot be developed in the filled region, where the product of the dispersion and nonlinearity coefficients becomes negative.

where p and q are the dispersion and nonlinearity coefficients. If $pq > 0$ and the contribution of the ϵ-order components is dominant, $W(x,t)$ is calculated as

$$W(x,t) = A_0 \mathrm{sech}\left\{\sqrt{\frac{q}{8p}} A_0 (x - U_g t)\right\} \cos\left\{kx - \left(\omega - \frac{qA_0^2}{8}\right) t\right\}, \quad (9)$$

where $A_0 = 2\epsilon A$. Furthermore, we observe that each mode can support a soliton-like pulse, and the soliton-like pulse carried by mode i ($i = 1, 2, 3, 4$) has voltage fraction R_i between lines 1 and 2. In general, because each mode can support soliton-like pulses, the nonlinear envelope pulse can preserve its original shape when it is carried by a specific mode. By applying the envelope pulses to both lines such that the voltage fraction of the incident pulses is equal to R_i, we can only develop the envelope pulses carried by mode i.

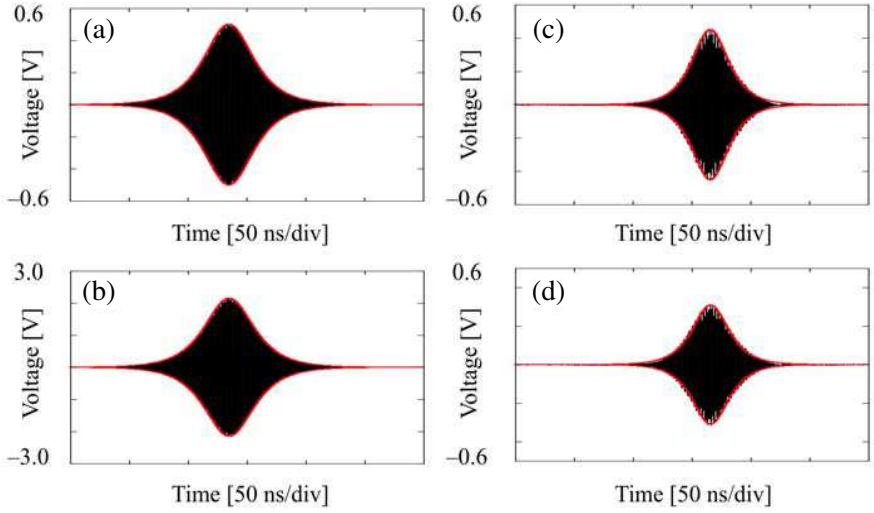

Figure 5. Soliton-like pulses on a coupled CRLH line. The waveforms of a pulse carried by mode 3 on lines 1 and 2 are shown in Figures 5(a) and (b), respectively. Figures 5(c) and (d) correspond to the waveforms of a pulse carried by mode 1 on lines 1 and 2, respectively. The numerically obtained waveforms and the analytically obtained envelope waveforms are shown by the black and red curves, respectively.

Instead of the explicit forms of p and q, in Figure 4, we show their pulse width and voltage fraction between lines 1 and 2 of a single bright soliton for the line parameters listed in Table 2. For the Schottky varactor, V_0, m_J, and V_J are set to -2.0 V, 2.0, and 2.0 V, respectively. The pulse width is calculated by Equation (9) such that the amplitude of the pulse on line 1 is 1.0, i.e., A_0 is set to R_i in Equation (9) for mode i ($i = 1, 2, 3, 4$). In Figure 4, the pulse width and the voltage fraction between the lines are shown by the red and blue curves, respectively. Moreover, the frequencies indicated by the dashed vertical lines represent the upper or lower cutoff frequencies shown in Figure 3. Because pq becomes negative, bright solitons cannot develop in the frequency range indicated in red. Note that modes 1 and 3 exhibit left-handedness, while modes 2 and 4 exhibit right-handed properties.

To validate the prediction of the NS equation, we numerically solved Equations (2)–(5) for the parameters listed in Table 2 with the same varactor model used to obtain Figure 4 by using the fourth-order Runge-Kutta method, and compared the resulting waveforms to Equation (9). The total number of cells was 2000. Figures 5(a) and (b)

show the waveforms monitored at the 500th cell on lines 1 and 2, respectively. We apply the envelope pulses with voltage fraction R_3 on lines 1 and 2; therefore, the envelope pulses are expected to be carried by mode 3. Note that the pulse must be distorted significantly after this long propagation unless the high dispersion is canceled by nonlinearity. The black curves show the numerically obtained waveforms, and the red curves show the analytically obtained ones for the 0.5-V amplitude on line 1 and the 1.3-GHz carrier frequency. The pulse width and the voltage fraction are correspondingly calculated to be 18.52 ns and -4.3, respectively. The numerically obtained waveforms are well characterized by the analytical ones. Similar calculations were performed for the nonlinear envelope pulses carried by mode 1. Applying the 1.30-GHz envelope pulses with voltage fraction R_1, we obtain Figures 5(c) and (d), which show the numerical and analytical waveforms on lines 1 and 2, respectively. The analytical envelope has the amplitude, pulse width, and voltage fraction of 0.45 V, 13.76 ns, and 0.7, respectively. Again, we confirm the pulse propagation without distortions and the significant similarity between the numerical and analytical envelope waveforms. It is observed that each mode supports non-distorted envelope pulses.

4. COLLISION OF TWO IDENTICAL NONLINEAR ENVELOPE PULSES IN COUPLED SCHOTTKY CRLH LINES

Here, we discuss the collision of two identical oppositely directing nonlinear envelope pulses along with the results of the time-domain calculations mentioned in the previous section. We again employ the parameters listed in Table 2. The total number of cells was set to 2000. The 1.3-GHz envelope pulses with voltage fraction R_3 were applied on both the left and right ends of lines 1 and 2. The pulses applied on both ends started to travel in opposite directions and collided at the midpoint. Figure 6 shows the results. Eight spatial waveforms are monitored on line 1 at even intervals. Time progresses downward with an increment of 32.8 ns. Both the incident pulses travel without distortion and collide at the fourth temporal point. As indicated by the red-dashed curves, a pair of envelope pulses is newly developed owing to the collision. The newly developed pulses are faster than the original ones. In addition, we observe that the carrier wave of the newly developed pulses has a considerably longer wavelength than that of the original ones. Figure 7 shows the temporal waveforms of the newly developed pulses that is recorded at the 500th cell. The waveforms on lines 1 and 2 are shown in Figures 7(a) and (b), respectively. The

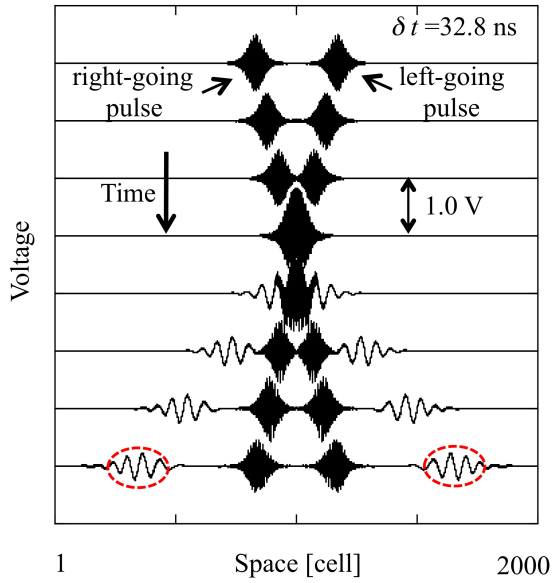

Figure 6. Collision of two identical nonlinear envelope pulses. Colliding pulses were carried by mode 3 and their carrier frequencies were set to 1.30 GHz. Time progresses downward with an increment of 32.8 ns.

carrier frequency is estimated to be 2.59 GHz by the spectral peak. In addition, the voltage fraction is estimated to be 0.42. At around 2.6 GHz, mode 1 is the specific mode that carries waves as shown in Figure 3. The voltage fraction of mode 1 is calculated to be 0.40. Thus, it is concluded that the newly developed pulses are carried by mode 1.

The positions of the fundamental, second, third harmonic waves are represented by P_1, P_2, P_3, respectively, in Figure 3. Moreover, either P_4 or P_4' corresponds to the fourth harmonic waves. We denote the wave vectors of the left- and right-going incident carrier waves as $\mathbf{k}_l$ and $\mathbf{k}_r$, respectively; therefore, the wave vector of newly developed carrier wave $\mathbf{k}_c$ has to satisfy the phase-matching condition: $\mathbf{k}_c \sim \mathbf{k}_n \equiv m_l\mathbf{k}_l + m_r\mathbf{k}_r$ for maximal amplitudes, where $m_{l,r}$ are the integers determined by the order of harmonics. For example, the development of the second harmonic envelope pulses requires $(m_r, m_l) = (1, 1)$. When the carrier frequency of the right-going pulse f_r is equal to that of the left-going pulse f_l, $\mathbf{k}_l$ becomes equal to $-\mathbf{k}_r$, $|\mathbf{k}_c|$ must be close to zero to develop the second harmonic envelope pulses. Similarly, we denote $|\mathbf{k}_l|$ $(= |\mathbf{k}_r|)$ as k_0; therefore, the phase-matching condition

requires $|\mathbf{k}_c| \sim k_0$ for the development of the third harmonic envelope pulses. Similarly, for the fourth harmonic envelope pulses, $|\mathbf{k}_c|$ must be close to either 0 or $2k_0$. We can see in Figure 3 that (a) the wave number corresponding to P_2 is close to zero, (b) the wave number of P_3 is definitely smaller than k_0, and (c) both the wave numbers of P_4 and P_4' are considerably smaller than $2k_0$ and sufficiently higher than zero. Thus, the newly developed pulses are carried by the second harmonic waves for the line parameters used in this study. As expected, the wavelengths of the collision-generated pulses are considerably longer than those of colliding pulses in Figure 6.

5. DISCUSSION

Both the left- and right-going pulses can be potentially develop by the collision. The balance of their amplitudes is determined by the wave vector that is closer to the phase-matched one. Without loss of generality, we only consider the case when $f_l \leq f_r$. When $f_l < f_r$, $\mathbf{k}_n$ directs to the right for the line parameters listed in Table 2 because (a) $|\mathbf{k}_r|$ becomes smaller than $|\mathbf{k}_l|$ and (b) both the incident pulses are carried by mode 3, which exhibits left-handedness. The sum-frequency pulses are carried by mode 1, which also exhibits left-handedness; therefore, the wave vector of the left-going collision-generated pulse ($\mathbf{k}_{cl}$) directs to the right, whereas that of the right-going pulse ($\mathbf{k}_{cr}$) directs to the left. When the separation between f_r and f_l becomes large, the right-going pulse must be significantly suppressed because $|\mathbf{k}_n - \mathbf{k}_{cr}|$ becomes sufficiently large to violate the phase-matching condition. As a result, the left-going pulse dominates the right-going one, as shown in Figure 7(a). When the frequency separation becomes small, $\mathbf{k}_n$ approaches zero; therefore, $|\mathbf{k}_n - \mathbf{k}_{cl}|$ and $|\mathbf{k}_n - \mathbf{k}_{cr}|$ become comparable. This suggests that the right-going collision-generated pulse tends to be comparable to the left-going one. Finally, these two become identical when $f_r = f_l$. To examine this, we perform several numerical calculations. The calculation setup is almost the same as that used to obtain the results in the previous section. We fix f_r at 1.30 GHz and f_l at the values slightly different values from 1.30 GHz. The results are shown in Figure 8. Figures 8(a) and (b) correspond to the cases when f_l was set to 1.32 and 1.28 GHz, respectively. The left-going pulse consistently becomes larger than the right-going one in Figure 8(a), and the amplitude balance is reversed in Figure 8(b). The spectrum peak of the newly developed pulses is at 2.61 and 2.57 GHz for the cases shown in Figures 8(a) and (b), respectively. They are supported by the sum-frequency carrier waves.

Finally, we consider the influence of losses. Because the wave

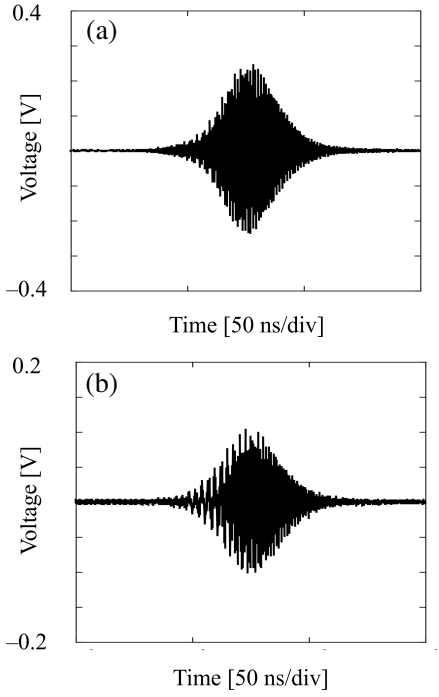

Figure 7. Waveforms of newly developed envelope pulses. The temporal waveforms monitored on lines 1 and 2 are shown in Figures 7(a) and (b), respectively.

losses are mainly caused by the parasitic resistances of inductors, the amplitude of the harmonic pulse for five different values of the resistances of L_{R1}, L_{L1}, L_{R2}, and L_{L2} is estimated. The resistance of L_{L1} was precisely set to $0.10\rho\,\Omega$, where fraction ρ was varied from 0.0 to 1.0 with 0.2 increments. For other inductors, we set the resistances proportional to the corresponding inductances. These values are practical for high-performance surface-mount inductors. Figure 9 shows the development of the second harmonic pulse for the input pulses having three different amplitudes by using temporal waveforms monitored at the 80th cell. Larger the losses, larger is the incident pulse decay; therefore, it is efficient to reduce the line's cell number for obtaining large amplitude of the newly developed pulses. We then set the total number of cells to 300. It is observed that the second harmonics amplitude decays exponentially as the resistances increase. Moreover, the ratio of the second harmonics amplitude for the 2.0-

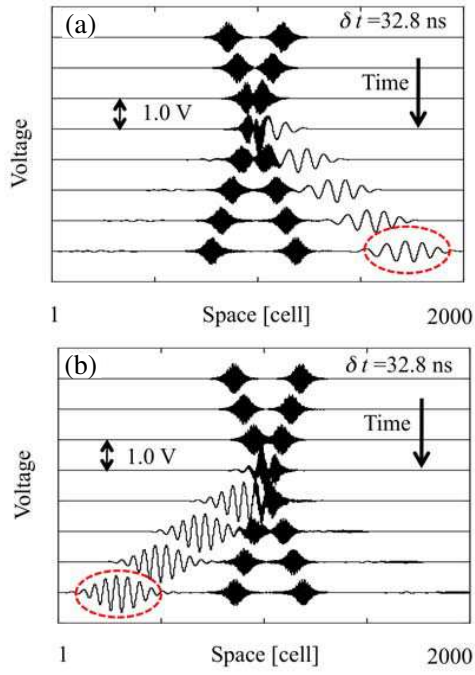

Figure 8. Collision of two nonlinear envelope pulses having different carrier frequencies. We fixed f_l at 1.30 GHz, while f_r were set to 1.32 and 1.28 GHz for Figures 7(a) and (b), respectively.

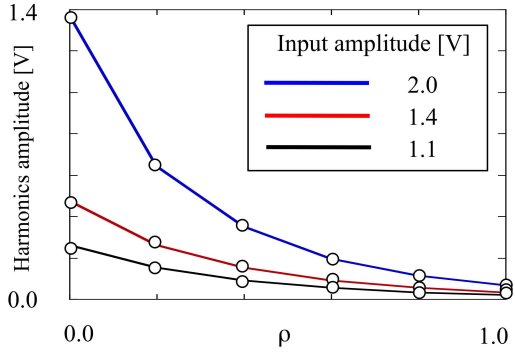

Figure 9. Influence of inductors' parasitic resistances. We set the resistances of L_{R1}, L_{L1}, L_{R2}, and L_{L2} to 0.048ρ, 0.06ρ, 0.10ρ, and $0.04\rho\,\Omega$, respectively, where the fraction ρ was varied from 0.0 to 1.0 with 0.2 increments.

V input to that for the 1.1-V input also decreases as ρ increases. The ratio is calculated to be 5.27 and 3.41 for the 2.0- and 1.1-V inputs, respectively. It is possible to obtain finite number of the second harmonic pulses even by using practical inductors. On the other hand, an amplification scheme must be devised for attenuation-free wave propagation. As mentioned above, we have investigated a TWFET, whose gate and drain transmission lines have a CRLH line structure [13]. It becomes important to examine the collision of nonlinear envelope pulses in TWFETs.

6. CONCLUSION

The properties of nonlinear envelope pulses developed in a coupled Schottky CRLH transmission line are investigated. Every mode can support nonlinear pulses. Moreover, the collision of two nonlinear envelope pulses leads to the development of a new pair of envelope pulses. Phase-matching essentially determines the carrier frequency and amplitude of the newly developed pulses. Although further investigations are required, we believe that the line may significantly increase the applications of the nonlinear envelope pulses.

REFERENCES

1. Caloz, C. and T. Itoh, *Electromagnetic Metamaterials: Transmission Line Theory and Microwave Applications*, Wiley-Interscience, New York, 2006.
2. Monti, G. and L. Tarricone, "Signal reshaping in a transmission line with negative group velocity behaviour," *Microwave Optical Technol. Lett.*, Vol. 51, 2627–2633, 2009.
3. Chi, P. and T. Itoh, "Dispersion engineering with CRLH metamaterials," *Proc. IEEE International Symposium on Radio-Frequency Integration Technology*, 128–131, 2009.
4. Gómez-Diaz, J. S., S. Gupta, A. Álvarez-Melcón, and C. Caloz, "Investigation on the phenomenology of impulse-regime metamaterial transmission lines," *IEEE Trans. Antennas and Propagat.*, Vol. 57, 4010–4014, 2009.
5. Kozyrev, A. B. and D. W. van der Weide, "Nonlinear wave propagation phenomena in left-handed transmission-line media," *IEEE Trans. Microwave Theory and Techniques*, Vol. 53, 238–245, 2005.

6. Gupta, S. and C. Caloz, "Dark and bright solitons in left-handed nonlinear transmission line metamaterials," *Proc. of IEEE MTT-S Int'l. Microwave Symp. 2007*, 979–982, Honolulu, 2007.
7. Kafaratzis, A. and Z. Hu, "Envelope solitons in nonlinear left handed transmission lines," *Proceedings of Metamaterials 2007*, 771–773, Rome, Oct. 22–24, 2007.
8. Simion, S., R. Marcelli, G. Bartolucci, G. Sajin, and F. Craciunoiu, "Nonlinear composite right/left-handed transmission line for frequency doubler and short pulse generation," *Proc. of Metamaterials 2008*, 492–494, 2008.
9. Gharakhili, F. G., M. Shahabadi, and M. Hakkak, "Bright and dark soliton generation in a left-handed nonlinear transmission line with series nonlinear capacitors," *Progress In Electromagnetics Research*, Vol. 96, 237–249, 2009.
10. Narahara, K., T. Nakamichi, T. Suemitsu, T. Otsuji, and E. Sano, "Development of solitons in composite right- and left-handed transmission lines periodically loaded with Schottky varactors," *J. Appl. Phys.*, Vol. 102, 024501–024504, 2007.
11. Ogasawara, J. and K. Narahara, "Short envelope pulse propagation in composite right- and left-handed transmission lines with regularly spaced Schottky varactors," *IEICE Electron. Express*, Vol. 6, 1576–1581, 2009.
12. Narahara, K., "Collision of nonlinear envelope pulses developed in composite right- and left-handed transmission lines periodically loaded with Schottky varactors," *Progress In Electromagnetics Research C*, Vol. 21, 1–21, 2011.
13. Narahara, K., "Nonlinear traveling-wave field-effect transistors for managing dispersion-free envelope pulses," *Progress In Electromagnetics Research Letters*, Vol. 23, 29–38, 2011.
14. Gupta, K. C., R. Garg, and I. J. Bahl, *Microstrip Lines and Slotlines*, Artech, 1979.
15. Taniuti, T., "Reductive perturbation method and far fields of wave equations," *Prog. Theor. Phys. Suppl.*, Vol. 55, 1–35, 1974.